Journal Pre-proof

Polarization-induced Ultrahigh Rashba Spin-orbit Interaction in ZnO/CdO Quantum Well

Mandun Fu, Minjiang Dan, Gongwei Hu, Lijie Li, Yan Zhang

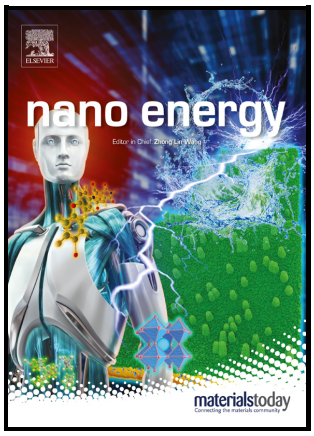

PII: S2211-2855(21)00565-6

DOI: https://doi.org/10.1016/j.nanoen.2021.106310

Reference: NANOEN106310

To appear in: *Nano Energy*

Received date: 13 May 2021
Revised date: 28 June 2021
Accepted date: 29 June 2021

Please cite this article as: Mandun Fu, Minjiang Dan, Gongwei Hu, Lijie Li and Yan Zhang, Polarization-induced Ultrahigh Rashba Spin-orbit Interaction in ZnO/CdO Quantum Well, *Nano Energy,* (2021) doi:https://doi.org/10.1016/j.nanoen.2021.106310

Polarization-induced Ultrahigh Rashba Spin-orbit Interaction in ZnO/CdO Quantum Well

Mandun Fu[1], Minjiang Dan[1], Gongwei Hu[1], Lijie Li[2,*] and Yan Zhang[1,3,4,*]

[1] School of Physics, University of Electronic Science and Technology of China, Chengdu 610054, China

[2] College of Engineering, Swansea University, Swansea, SA1 8EN, UK

[3] Beijing Institute of Nanoenergy and Nanosystems, Chinese Academy of Sciences; Beijing 100083, China

[4] College of Nanoscience and Technology, University of Chinese Academy of Sciences, Beijing 100049, China

*To whom correspondence should be addressed, E-mail: zhangyan@uestc.edu.cn and L.Li@swansea.ac.uk

Abstract

Spin-orbit interaction (SOI) connecting an electronic spin with its momentum is crucial for numerous fundamental physical researches and their applications, including quantum spin Hall effect, Majorana Fermions and spin-orbit qubits. By breaking structural inversion symmetry, Rashba spin-orbit interaction (RSOI) provides an available method for the manipulation of spin by controlling electronic movement within external potential field. In this study, we demonstrate the RSOI of conduction electron modulated by stress-induced polarization field in ZnO/CdO quantum well (QW). The polarization field exactly triggers band inversion between the electron and light hole. The peak of RSOI coefficient can reach approximately up to 83 meV · nm, almost three orders of magnitude higher than the conventional GaAs-based QWs. This study can be beneficial to sufficient manipulation of spin qubits by strong RSOI quantum piezotornic effect induced, and will stimulate an intense researching interest in low-dimensional quantum piezotronic devices.

Graphical Abstract

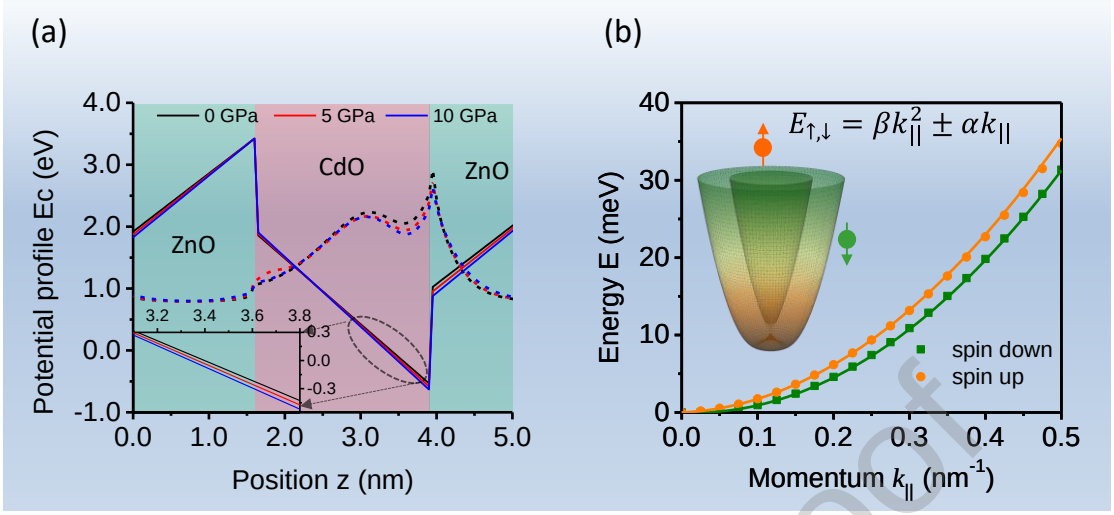

Keywords: Quantum piezotronics, Rashba spin-orbit interaction, stress-induced polarization field, ZnO/CdO quantum well

1. Introduction

Piezotronic and piezo-phototronic devices based on third-generation semiconductors and two-dimensional materials have greatly advanced the rapid development of multifunctional nanodevice applications, flexi-electronics and self-powered systems. Based on ZnO, GaN and monolayer MoS_2, various high performance devices have been developed including nanogenerators [1, 2], piezotronic field effect transistors [3], high sensitivity piezotronic strain sensors [4], taxel-addressable matrices devices [5] and quantum piezotronic devices [6-8]. By the coupling of piezoelectricity, semiconductor and light excitation, the carriers generation/recombination and transport properties can be controlled by strain-induced piezo-charges in the interface or junction regions of heterostructure [9, 10]. High-resolution pressure imaging devices have been fabricated by the integrated array of nanowires light-emitting diode strain sensors [11].

Piezotronic and piezo-phototronic effects can effectively enhance the performance of sensors, switches and actuators due to ultrahigh field in junctions and contacts. For example, piezotronic high sensitivity oxygen sensors were developed based on ZnO nanowire [12]. The photocurrent in ZnO/Au Schottky junction UV detector showed a 440% enhancement by the

piezotronic effect [13]. Pressure sensor matrix based on ZnS:Mn mechanoluminescence particles has demonstrated pressure recording and mapping from 0.6 to 50 MPa [14]. The ON/OFF ratio of piezotronic logic nanodevices based on InN/GaN topological insulator have reached over 10^{10} [15].

Spin quantum bit (qubit) plays an important role in quantum information processing and quantum computing [16, 17]. The prerequisite to produce spin qubits in the materials is spin-orbit interaction (SOI), and its electrical manipulation is correlated with Rashba-type SOI (RSOI) due to the breaking structural inversion symmetry. The RSOI coefficient can enhance Rabi frequency which is a key performance indicator to estimate the manipulating speed of spin qubits in devices[18, 19]. For example, the Rabi frequency increases linearly with the RSOI coefficient under same external conditions and the rotating speed of spin qubit in ZnO/CdO QW increases from 0.19 MHz to 4.05 MHz by applying stress. The coherent transitions (Rabi oscillations) between spin-up and spin-down with 90° rotations are as fast as ~63 nanoseconds which is on the same order of magnitude as the time in GaAs quantum dot [20].

Quantum piezotronics have great potential for designing or improving performances of quantum materials and devices. Strain-induced piezopotential has been used to tune Rashba spin-orbit interaction (RSOI) in ZnO/P3HT nanowire array structure at room temperature [21]. By interplaying the electron spin and its momentum, spin-orbit interaction (SOI) plays an important role in the fundamental researches of condensed matter physics and the novel applications of quantum materials and devices [22, 23]. In GaAs/AlGaAs quantum dots (RSOI coefficient ~ 0.1 meV · nm) and InAs nanowires (RSOI coefficient ~ 0.2 meV · nm) [24, 25], spin-orbit qubits can be established by manipulating individual electron spin within an oscillating SOI field for quantum information processing [26, 27]. The gate-controlled RSOI coefficient in parabolic GaAs/AlGaAs is less than 0.1 meV · nm due to electric field ~1 KV/cm [28]. RSOI coefficient is ~ 0.3 meV · nm in a polar GaN/InGaN quantum wells (QWs) due to the polarization field ~ 2.0 MV/cm [29]. Therefore, quantum piezotronics offers an effective way for new heterostructures with large RSOI coefficients, which may overcome the challenge of the RSOI limitation for new topological classes of materials and spin qubit applications. Polarization-induced large RSOI coefficients also give a method for greater spin

current in spin Hall device [30] and smaller size of spin-field-effect transistor [31]

In this paper, we explore the novel device structures of ultrahigh RSOI induced by the polarization field in ZnO/CdO QWs quantum piezotronic devices. Wurtzite ZnO QWs are important quantum materials to study integer/fractional quantum Hall effects and topological insulators [7, 32, 33]. The QW with three layers ZnO and four layers CdO shows a record high RSOI coefficient ~ 83 meV · nm assisted by the quantum piezotronic effect, which is around 16.6 times higher than the reported value. Such high RSOI coefficient arises from the combining effect of band inversion and the coupling between the electron and light hole. These two effects also lead to an interesting peak for the RSOI coefficient, depending on the QW width.

2. Theory and Methods

Wurtzite ZnO can be synthesized with controllable properties [34, 35]. By using the high quality grown of metal oxides heterostructure, integral and fractional quantum Hall effects in ZnO QWs have been successfully observed in experiment [32, 36]. Room-temperature electron spin dynamics has also been widely studied in the thin film and quantum dot of wurtzite ZnO [37, 38]. A big challenge for fabrication of ZnO/CdO QWs is that the thermodynamically-stable crystalline phases of the CdO are rocksalt, not wurtzite [39]. Defect control in ZnO is also difficult in the fabrication of ZnO/CdO QWs. High quality ZnO quantum well can be achieved by ozone-assisted molecular beam epitaxy and pulsed laser deposition [32, 40], and high quality ZnO/CdO QWs can be synthesized by nonequilibrium laser plasma ablation when a very thin CdO is deposited on ZnO interlayers to sustain its wurtzite phase [41]

Here, we demonstrate the RSOI modulated by the stress-induced polarization field of ZnO/CdO QWs. The QW is selected as our studying target because polarization field can drive a topological phase transition with a stress-dependent band inversion [42]. Band inversion can bring in strong electron-hole coupling to obtain large SOI. In order to account for electron-hole coupling, theoretically we start from an eight-band Kane Hamiltonian of wurtzite material which is given by [43, 44]

$$H = \begin{pmatrix} G(k) & \Gamma \\ -\bar{\Gamma} & \bar{G}(k) \end{pmatrix} \tag{1}$$

where G and Γ are 4×4 matrices with the complex conjugate $\bar{G}$ and $\bar{\Gamma}$, respectively. The explicit expression of equation (1) can be found in Ref. [43, 44]. By solving Schrödinger equation $[H(k)+V(z)]\psi_n(z) = E_n\psi_n(z)$ over a single QW under periodic boundary condition, one can obtain band dispersion of interest subbands (here it is the first conduction band C1 including spin). Here, $\psi_n(z)$ is the wave function, E_n is the energy level and $V(z)$ is the potential arising from the polarization.

For a strained QW grown along *c*-axis direction, piezoelectric polarization is obtained from $P^{piezo} = e_{33}s_{33} + e_{31}(s_{11}+s_{22})$, where s_{11}, s_{22} and s_{33} are the strains along *x*, *y* and *z* axis (*c* axis) direction, e_{33} and e_{31} are the components of piezoelectric coefficient. The strain comes from lattice misfit among different materials and the externally applied stress $S = C^{-1}\cdot\sigma$, C is elastic coefficient, S is strain tensor and σ is stress tensor. Total polarization consists of spontaneous and piezoelectric portion $P_{w,b} = P^{sp}_{w,b} + e_{33,w,b}s_{33,w,b} + e_{31,w,b}(s_{11,w,b}+s_{22w,b})$, where the subscript w and b respectively label the quantity in the well and barrier layer. The polarization field can then be given by [45] $F_j = \left[\sum_{k=w,b}\left(P_k - P_j\right)W_k/\varepsilon_k\right] \Big/ \left(\varepsilon_0\varepsilon_j\sum_{k=w,b}W_k/\varepsilon_k\right)$, where the subscript $j = w \text{ or } b$, W is the width, ε_0 and $\varepsilon_{j,k}$ are vacuum and relative dielectric constants. The potential can be obtained $V(z) = \begin{cases} zF_w, & well \\ W_wF_w + (z-W_w)F_b, & barrier \end{cases}$. Notice that we here focus mainly on the RSOI coefficient but not on the explicit spin splitting energy, which is much more natural and widely studied in experiment [28, 29, 46, 47]. This indicates that it does not need to know Fermi wave vector or the doping, and for the sake of simplicity we do not consider doping in this study. The electrons can screen the polarization in quantum devices depending on the doping concentration [48], the screening effect can also be neglected.

Rabi oscillations are coherent transitions between spin-up and spin-down with 90° rotations in qubits, the changing speed of this oscillations can be expressed in terms of the Rabi frequency. The RSOI coefficient can linearly affect the Rabi frequency which is an important indicator of qubit performance. The Rabi frequency is given as [20].

$$f_{Rabi} = (g\mu_B \left|B_{eff}\right|) / 2h \tag{2}$$

where g represents the g factor, μ_B is the Bohr magneton, h is Planck's constant and B_{eff} is effective magnetic field. The effective magnetic field $\left|B_{eff}(t)\right| = 2\left|B_{ext}\right|\frac{l_{dot}}{l_{SO}}\frac{e\left|E(t)\right|l_{dot}}{\Delta}$, with spin-orbit length l_{SO}, orbital energy splitting Δ, electric field $\left|E(t)\right|$, and the external magnetic field B_{ext}. Here, $l_{dot} = \hbar / \sqrt{m^*\Delta}$ and $l_{SO}^{-1} = m^*(\alpha \mp \beta)/\hbar$ with effective electron mass m^*, the reduced Planck constant $\hbar$, Rashba spin-orbit interaction coefficient α, and Dresselhaus spin-orbit interaction coefficient β. For the external magnetic field $\left|B_{ext}\right| = hf_{ac} / g\mu_B$, f_{ac} is the excitation frequency. The Rabi frequency can be derived as a function of Rashba spin-orbit interaction coefficient:

$$f_{Rabi} = \frac{(\alpha \mp \beta)}{\Delta^2}\hbar e\left|E\right| f_{ac} \tag{3}$$

where the orbital energy splitting Δ is a constant of materials, electric field E and excitation frequency f_{ac} are applied by external experiment environment.

3. Results and discussions

Fig. 1(a) shows potential profile and wave function of the first electronic subband *C*1 in single ZnO/CdO QW along *c*-axis direction under [010] stress. The widths of ZnO barrier and CdO well are 2.6 nm (5 layers) and 2.3 nm (4 layers), respectively. Wave function corresponds to the *C*1 at the center of Brillouin region, i.e., $k_x = k_y = 0$. Under different stresses, potential profile has a tiny change and occurs mainly at the right interface between ZnO and CdO, as seen in the insert of Fig. 1(a). This tiny change in potential is due to stress-induced piezoelectric polarization enhancing electric field of the QW, and modifies the

QW asymmetry. As a result, wave function of the *C*1 has slight variations but, as it is shown below that it can bring in significant influence on the RSOI. The considerable difference of conduction effective mass between ZnO (~ $0.18m_0$) and CdO (~ $0.15m_0$) and narrow band gap makes wave functions severely deformed at the interface [49].

Knowledge of energy levels and wave functions at $k_x = k_y = 0$ allows for constructing a low-dimensional effective Hamiltonian to estimate the RSOI intensity. By using Löwdin perturbation method, we can obtain a low-dimensional effective 2×2 Hamiltonian $H_{2D} = (E_0 + \beta k_{\parallel}^2)\boldsymbol{I}_{2\times 2} + \alpha(k_x\sigma_y - k_y\sigma_x)$ under basis $\{|C1,\uparrow\rangle, |C1,\downarrow\rangle\}$, where $k_{\parallel} = \sqrt{k_x^2 + k_y^2}$, $\mathbf{I}_{2\times 2}$ is a 2×2 identity matrix, σ_x and σ_y are Pauli matrices, β is effective mass parameter and α is the RSOI coefficient to measure the intensity of Rashba spin splitting. This effective Hamiltonian is valid when the electron momentum or wave vector *k* is small ($ak/2\pi \ll 1$ throughout this work, $a = 0.2$ nm is lattice constant).

Fig. 1(b) shows spin-resolved band dispersion of the *C*1 without externally applied stress. Spin splitting can be observed due to large SOI originated from the presence of intrinsic polarization field. From above effective Hamiltonian, we can analytically give band dispersion for up and down spin $E_{\uparrow,\downarrow} = \beta k_{\parallel}^2 \pm \alpha k_{\parallel}$, where $\beta = 137$ meV · nm^2 and $\alpha = 4.51$ meV · nm. Fig. 1(b) shows a good agreement between the analytical results and eight-band Kane model, indicating validity of the effective Hamiltonian. The insert displays three-dimensional view of spin-resolved band structure of the *C*1, which exhibits the typical feature of Rashba spin splitting (described below).

In the following, we start to turn to the case with a stress-induced band inversion. The stress-induced piezoelectric polarization can tune the built-in electric field of ZnO/CdO QW and further control the Rashba SOC. For intuitively illustrating RSOI coefficient, we display three-dimensional view of band dispersion at $\sigma = 4$, 6 and 8 GPa in Fig. 2(a). The RSOI coefficient is 7.9 meV · nm ($\sigma = 4$ GPa) in A, 13.2 meV · nm ($\sigma = 6$ GPa) in B and 4.0 meV · nm ($\sigma = 8$ GPa) in C. All the cases clearly show spin splitting, and one can easily judge spin splitting energy meeting $\Delta E_2 > \Delta E_1 > \Delta E_3$, where ΔE_1, ΔE_2 and ΔE_3 are the splitting energy at stress $\sigma = 4$, 6 and 8 GPa, respectively. Actually, spin splitting energy can

be calculated from $\Delta E = 2\alpha k_{\parallel}$, which is 3.2, 5.3 and 1.6 meV at $k_{\parallel} = 0.2$ nm^{-1} for $\sigma = 4$, 6 and 8 GPa, respectively. Here, we can clearly see the typical feature of Rashba spin splitting which is down-spin band exhibiting a non-monotonic *k* dependence (first decreases and then increases with *k*). The minimum energy for down-spin electron occurs at wave vector $k_{\parallel} = \alpha / \beta$. By contrast, the up-spin state displays the usual parabolic dispersion.

Fig. 2(b) shows stress-dependent polarization field in the barrier and well layer. Their field intensity increases linearly with stress, and the slope is approximately 0.057 and -0.064 MV/cm $\cdot$ GPa^{-1} for the well and barrier layer, respectively. The positive and negative sign of polarization field stands for the opposite directions.

Fig. 2(c) shows the RSOI coefficient of the *C*1 as a function of stress. A striking feature is the appearance of a peak RSOI coefficient $\alpha = 19.5$ meV $\cdot$ nm at the critical stress $\sigma_c = 6.6$ GPa. This critical stress occurs at band inversion between the *C*1 and *L*1 (the first light-hole subband) but not between the *C*1 and *H*1 (the first heavy-hole subband) although the latter occurs first at $\sigma = 5.5$ GPa, as seen in the inset of Fig. 2(c). This indicates that RSOI coefficient has direct connection with coupling between the *C*1 and *L*1. Actually, according to the second-order perturbation theory the RSOI coefficient can be written as [50] $\alpha = \xi_z \langle \psi_{L1} | H' | \psi_{C1} \rangle | \varepsilon_{L1} - \varepsilon_{C1} |^{-1}$, where ξ_z is electrical field to bring in structural inversion asymmetry, H' is perturbation Hamiltonian, ψ_{L1} and ψ_{C1} are wave functions, ε_{L1} and ε_{C1} are energy levels for the *C*1 and *L*1. This expression can give a qualitative explanation for peak behavior of RSOI. When the stress increases to tune energy level of the *C*1 gradually close to the *L*1 [see the insert of Fig. 2(c)], RSOI coefficient grows rapidly and reach a maximum at σ_c. Because the coupling between the *C*1 and *L*1 is strong at $k_{\parallel} = 0$, a nonzero gap $\Delta = \min\left(|\varepsilon_{L1} - \varepsilon_{C1}|\right)$ appears. This gap ensures a large but not infinite α value. For the stress exceeding σ_c, energy level of the *C*1 starts to keep away from the *L*1, giving rise to a sharply decreasing RSOI coefficient, as shown in Fig. 2(c). Although the *C*1 can fully intersect with the *H*1 at $\sigma = 5.5$ GPa, zero coupling $\langle \psi_{H1} | H' | \psi_{C1} \rangle = 0$ always exists among them, giving rise to no contribution of the *H*1 to α. A similar phenomenon can

also be presented in GaN/InN QW and the peak occurs at band inversion among the *C*1 and *L*1, as seen in Fig. 2(d) and its insert.

Considering polarization field being strongly dependent on the QW width, we show the max RSOI coefficient for different ZnO/CdO quantum wells in Fig. 3(a). The RSOI coefficients in structures with band inversion are far greater than those structures without band inversion. The RSOI coefficient at different layer number of ZnO under a fixed 4-layers CdO has been shown in Fig 3(b). A common peak phenomenon can be seen at critical stress of 1.1, 6.6, 10.9 and 15 GPa for six to three layers ZnO. It has been confirmed that all these peaks appear at band inversion between the *C*1 and *L*1. Interestingly, the peak RSOI coefficient increases with the growing of barrier width, and the maximum can reach up to 82.7 meV · nm at 3-layer ZnO width. The increasing peak is due to the decreasing of *C*1-*L*1 gap Δ by reducing barrier width.

We have compared RSOI coefficient of ZnO/CdO QWs with other QW systems in Table I. ZnO/CdO QW exhibits the tremendous superiority in the modulation of Rashba spin splitting, and its amplitude is almost three orders higher than the conventional GaAs QWs. The latter is to use gate voltage to induce Rashba spin splitting. The results in Table I also follows our conclusion that the amplitude of RSOI coefficient is inversely proportional to band gap of the QWs because of $E_G^{GaAs} > E_G^{GaN} > E_G^{InGaN} > E_G^{InAs} > E_G^{CdO}$.

Fig. 4 displays another case for piezotronic effect regulating Rashba spin-orbit interaction coefficient in (a) ZnO/MgO QWs and (b) AlN/GaN QWs with a wide gap, which are so wide that strong polarization field cannot drive band inversion. In this situation, the manipulation of Rashba SOC coefficient by stress is extremely poor, as shown in Fig. 4. There are two conditions under which a strong RSOI may occur in a heterostructure QW, i.e. consisting of a material having a narrower bandgap and a material exhibiting relatively strong strain induced polarization.

4. Conclusion

In summary, we explore the impact of stress-induced polarization field on the RSOI for conduction electrons in ZnO/CdO QWs. The RSOI coefficient exhibits a peak phenomenon

with the increasing of polarization field. Such peak stems from band inversion among the electron and light hole, and can reach as high as 83 meV · nm. This kind of peak phenomenon for RSOI coefficient exists intrinsically in these systems with structural asymmetry-induced band inversion, and has further been verified in InN/GaN QWs. This study opens an avenue for the manipulation of spin qubits. Control of qubits spin states relies on the electric field and AC voltage burst for quantum dot. The initialized state is a spin-blockade regime with two same spin-state electrons and the qubit readout and initialization rely on the effect of spin blockade [51].

Reference

1. Wang, Z.L. and J. Song, *Piezoelectric nanogenerators based on zinc oxide nanowire arrays.* Science, 2006. **312**(5771): p. 242-6.
2. Qin, Y., X. Wang, and Z.L. Wang, *Microfibre–nanowire hybrid structure for energy scavenging.* Nature, 2008. **451**(7180): p. 809-813.
3. Wang, X., et al., *Piezoelectric Field Effect Transistor and Nanoforce Sensor Based on a Single ZnO Nanowire.* Nano Letters, 2006. **6**(12): p. 2768-2772.
4. Wu, W., Y. Wei, and Z.L. Wang, *Strain-gated piezotronic logic nanodevices.* Adv Mater, 2010. **22**(42): p. 4711-5.
5. Wu, W., X. Wen, and Z.L. Wang, *Taxel-addressable matrix of vertical-nanowire piezotronic transistors for active and adaptive tactile imaging.* Science, 2013. **340**(6135): p. 952-7.
6. Hu, G., et al., *Piezotronic Transistor Based on Topological Insulators.* ACS Nano, 2018. **12**(1): p. 779-785.
7. Hu, G. and Y. Zhang, *Quantum piezotronic devices based on ZnO/CdO quantum well topological insulator.* Nano Energy, 2020. **77**.
8. Liu, R., et al., *Piezotronic spin and valley transistors based on monolayer MoS2.* Nano Energy, 2020. **72**.
9. Zhang, Y., Y. Liu, and Z.L. Wang, *Fundamental theory of piezotronics.* Adv Mater, 2011. **23**(27): p. 3004-13.
10. Zhang, Y., et al., *Theory of piezotronics and piezo-phototronics.* MRS Bulletin, 2018. **43**(12): p. 928-935.
11. Pan, C., et al., *High-resolution electroluminescent imaging of pressure distribution using a piezoelectric nanowire LED array.* Nature Photonics, 2013. **7**(9): p. 752-758.
12. Niu, S., et al., *Enhanced performance of flexible ZnO nanowire based room-temperature oxygen sensors by piezotronic effect.* Adv Mater, 2013. **25**(27): p. 3701-6.
13. Lu, S., et al., *Piezotronic interface engineering on ZnO/Au-based Schottky junction for enhanced photoresponse of a flexible self-powered UV detector.* ACS Appl Mater Interfaces, 2014. **6**(16): p. 14116-22.
14. Wang, X., et al., *Dynamic pressure mapping of personalized handwriting by a flexible sensor matrix based on the mechanoluminescence process.* Adv Mater, 2015. **27**(14): p. 2324-31.
15. Dan, M., et al., *High performance piezotronic logic nanodevices based on GaN/InN/GaN topological insulator.* Nano Energy, 2018. **50**: p. 544-551.
16. Imamog¯lu, A., et al., *Quantum Information Processing Using Quantum Dot Spins and Cavity QED.* Physical Review Letters, 1999. **83**(20): p. 4204-4207.
17. Loss, D. and D.P. DiVincenzo, *Quantum computation with quantum dots.* Physical Review A, 1998. **57**(1): p. 120-126.
18. Flindt, C., A.S. Sorensen, and K. Flensberg, *Spin-orbit mediated control of spin qubits.* Phys Rev Lett, 2006. **97**(24): p. 240501.
19. Rashba, E.I. and A.L. Efros, *Orbital mechanisms of electron-spin manipulation by an electric field.* Phys Rev Lett, 2003. **91**(12): p. 126405.
20. Nowack, K.C., et al., *Coherent control of a single electron spin with electric fields.* Science, 2007. **318**(5855): p. 1430-3.
21. Zhu, L., et al., *Piezotronic Effect on Rashba Spin–Orbit Coupling in a ZnO/P3HT Nanowire Array Structure.* ACS Nano, 2018. **12**(2): p. 1811-1820.

22. Galitski, V. and I.B. Spielman, *Spin-orbit coupling in quantum gases.* Nature, 2013. **494**(7435): p. 49-54.
23. Manchon, A., et al., *New perspectives for Rashba spin-orbit coupling.* Nat Mater, 2015. **14**(9): p. 871-82.
24. Valín-Rodríguez, M., A. Puente, and L. Serra, *Quantum dots based on spin properties of semiconductor heterostructures.* Physical Review B, 2004. **69**(15).
25. Takase, K., et al., *Highly gate-tuneable Rashba spin-orbit interaction in a gate-all-around InAs nanowire metal-oxide-semiconductor field-effect transistor.* Sci Rep, 2017. **7**(1): p. 930.
26. Nowack, K.C., et al., *Coherent Control of a Single Electron Spin with Electric Fields.* Science, 2007. **318**(5855): p. 1430.
27. Nadj-Perge, S., et al., *Spin–orbit qubit in a semiconductor nanowire.* Nature, 2010. **468**(7327): p. 1084-1087.
28. Studer, M., et al., *Gate-Controlled Spin-Orbit Interaction in a ParabolicGaAs/AlGaAsQuantum Well.* Physical Review Letters, 2009. **103**(2).
29. Litvinov, V.I., *Polarization-induced Rashba spin-orbit coupling in structurally symmetric III-nitride quantum wells.* Applied Physics Letters, 2006. **89**(22): p. 222108.
30. Sheng, L., D.N. Sheng, and C.S. Ting, *Spin-Hall effect in two-dimensional electron systems with Rashba spin-orbit coupling and disorder.* Phys Rev Lett, 2005. **94**(1): p. 016602.
31. Sugahara, S. and J.J.P.o.t.I. Nitta, *Spin-transistor electronics: An overview and outlook.* 2010. **98**(12): p. 2124-2154.
32. Tsukazaki, A., et al., *Quantum Hall effect in polar oxide heterostructures.* Science, 2007. **315**(5817): p. 1388-1391.
33. Tsukazaki, A., et al., *Observation of the fractional quantum Hall effect in an oxide.* Nat Mater, 2010. **9**(11): p. 889-93.
34. Joo, J., et al., *Face-selective electrostatic control of hydrothermal zinc oxide nanowire synthesis.* Nat Mater, 2011. **10**(8): p. 596-601.
35. Wei, Y., et al., *Wafer-scale high-throughput ordered growth of vertically aligned ZnO nanowire arrays.* Nano Lett, 2010. **10**(9): p. 3414-9.
36. Falson, J. and M. Kawasaki, *A review of the quantum Hall effects in MgZnO/ZnO heterostructures.* Reports on Progress in Physics, 2018. **81**(5): p. 056501.
37. Liu, W.K., et al., *Room-Temperature Electron Spin Dynamics in Free-Standing ZnO Quantum Dots.* Physical Review Letters, 2007. **98**(18).
38. Ghosh, S., et al., *Room-temperature spin coherence in ZnO.* Applied Physics Letters, 2005. **86**(23): p. 232507.
39. Zhu, Y.Z., et al., *Electronic structure and phase stability of MgO, ZnO, CdO, and related ternary alloys.* Physical Review B, 2008. **77**(24).
40. Jiang, J., et al., *Structural and optical properties of ZnCdO/ZnO multiple quantum wells grown on sapphire substrates using pulsed laser deposition.* Journal of Applied Physics, 2012. **112**(8).
41. Ashrafi, A. and K. Ostrikov, *Raman-active wurtzite CdO nanophase and phonon signatures in CdO/ZnO heterostructures fabricated by nonequilibrium laser plasma ablation and stress control.* Applied Physics Letters, 2011. **98**(13).
42. Hu, G. and Y. Zhang, *Quantum piezotronic devices based on ZnO/CdO quantum well topological insulator.* Nano Energy, 2020. **77**: p. 105154.
43. Winkelnkemper, M., A. Schliwa, and D. Bimberg, *Interrelation of structural and electronic*

properties inInxGa1−xN ／GaNquantum dots using an eight-bandk·pmodel. Physical Review B, 2006. **74**(15).

44. Gershoni, D., C.H. Henry, and G.A. Baraff, *Calculating the optical properties of multidimensional heterostructures: Application to the modeling of quaternary quantum well lasers.* IEEE Journal of Quantum Electronics, 1993. **29**(9): p. 2433-2450.
45. Ridley, B.K., W.J. Schaff, and L.F. Eastman, *Theoretical model for polarization superlattices: Energy levels and intersubband transitions.* Journal of Applied Physics, 2003. **94**(6): p. 3972-3978.
46. Belyaev, A.E., et al., *Investigation of spin-orbit interaction inAlGaN ／GaNheterostructures with large electron density.* Physical Review B, 2008. **77**(3).
47. Cimpoiasu, E., et al., *Effect of illumination on the interplay between Dresselhaus and Rashba spin-orbit couplings in InAs quantum wells.* Journal of Applied Physics, 2019. **126**(7): p. 075704.
48. Di Carlo, A., et al., *Doping screening of polarization fields in nitride heterostructures.* Applied Physics Letters, 2000. **76**(26): p. 3950-3952.
49. Ma, X., et al., *Stable finite element method of eight-band k·p model without spurious solutions and numerical study of interfaces in heterostructures.* Journal of Applied Physics, 2014. **116**(23): p. 235702.
50. Rothe, D.G., et al., *Fingerprint of different spin–orbit terms for spin transport in HgTe quantum wells.* New Journal of Physics, 2010. **12**(6): p. 065012.
51. Hanson, R., et al., *Spins in few-electron quantum dots.* Reviews of Modern Physics, 2007. **79**(4): p. 1217-1265.
52. Studer, M., et al., *Gate-controlled spin-orbit interaction in a parabolic GaAs/AlGaAs quantum well.* Phys Rev Lett, 2009. **103**(2): p. 027201.
53. Fu, J., et al., *Spin-orbit coupling in wurtzite heterostructures.* Physical Review B, 2020. **101**(13).

Figure captions

Fig. 1. (a) Potential profile (solid line) and wave function (dotted line) of the *C*1 in single ZnO/CdO QW under different stresses. (b) Spin-dependent band dispersion of the E1 at $\sigma = 0$ GPa. The wave function is calculated from eight-band Kane model, and the band dispersion, where $\beta = 137$ meV · nm^2, and $\alpha = 4.51$ meV · nm. The insert shows three-dimensional view of band dispersion for up and down spin. In the QW, the widths of ZnO barrier and CdO well are 2.6 nm (5 layers) and 2.3 nm (4 layers), respectively.

Fig. 2. (a) A, B, C are subband dispersions at stress $\sigma = 4$, 6 and 8 GPa, respectively. (b) Polarization field of well and barrier layer in ZnO/CdO QW versus stress. Rashba SOC coefficient versus stress in (c) ZnO/CdO QW and (d) GaN/InN QW. Blue dashed line stands for the critical stress in (c) $\sigma_c = 6.6$ GPa and in (d) $\sigma_c = 8.5$ GPa. The inset shows subband C1 (first conduction), H1 (first heavy hole) and L1 (first light hole) against stress at $k_{\|} = 0$. The width of ZnO barrier and CdO well are 3.1 nm (6 layers) and 1.7 nm (3 layers), and the width of GaN barrier and InN well are 1.5 nm (3 layers) and 3.5 (6 layers) nm respectively.

Fig. 3. (a) The max Rashba SOC coefficient for different ZnO/CdO QWs. (b) Stress-dependent Rashba SOC coefficient at different ZnO layers. The width of CdO is fixed at 2.3 nm (4 layers), and ZnO barrier layer varies from 1.6 to 3.1 nm (3 to 6 layers), corresponding to critical stress of 1.1, 6.6, 10.9 and 15 GPa, respectively.

Fig. 4. Rashba SOC coefficient versus stress in (a) ZnO/MgO QWs and (b) AlN/GaN QWs.

Table I. The first-order RSOI coefficient in different QWs

Figures

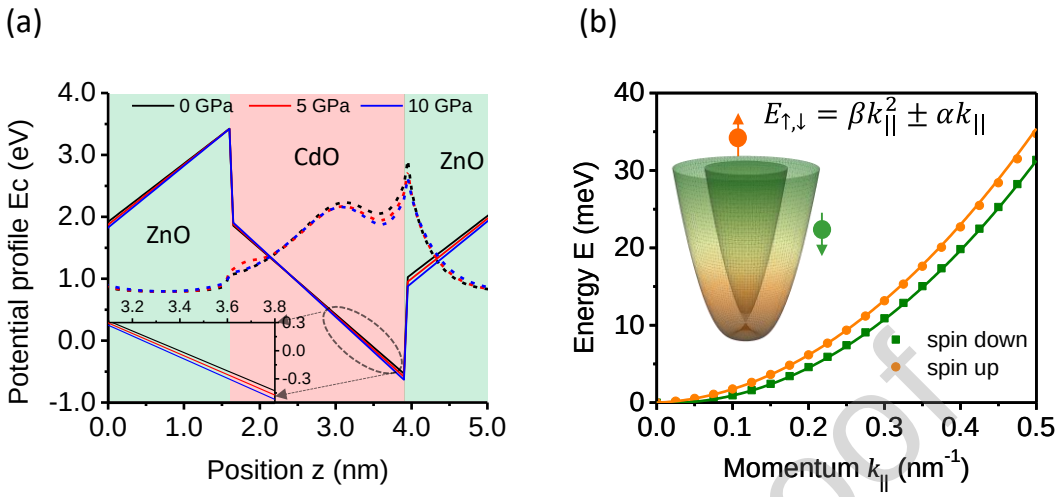

Figure 1

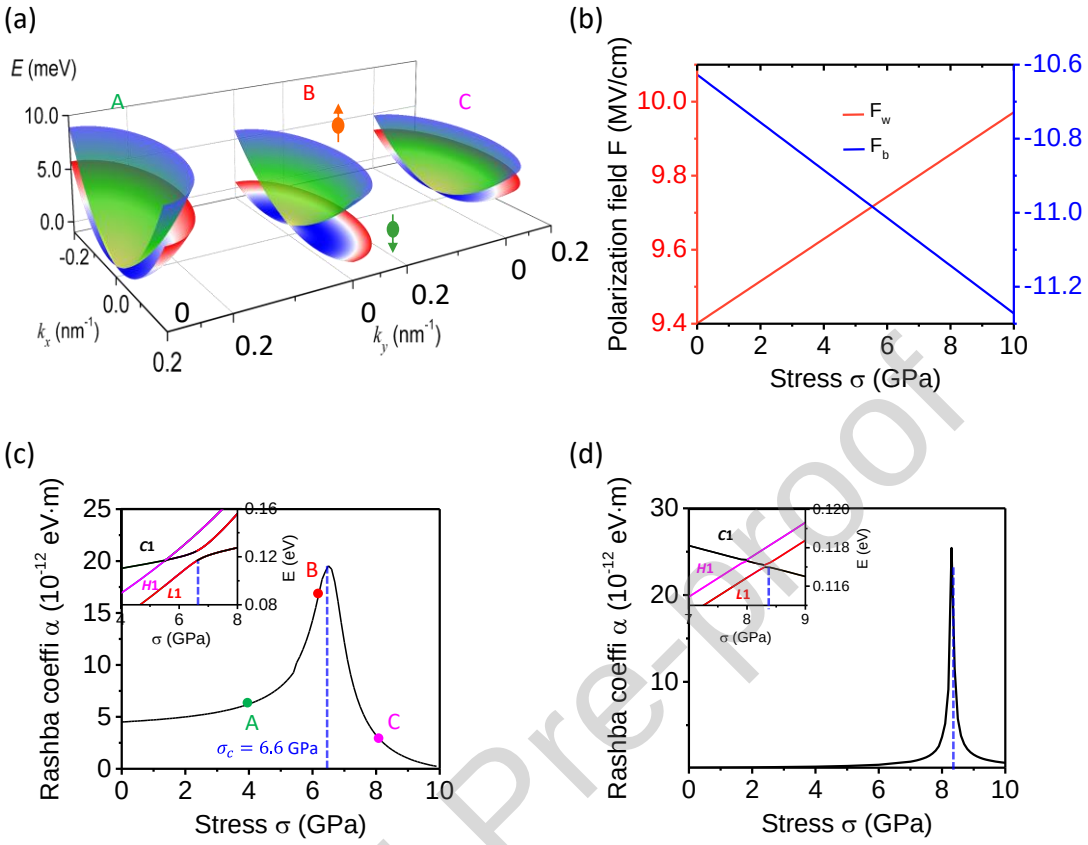

Figure 2

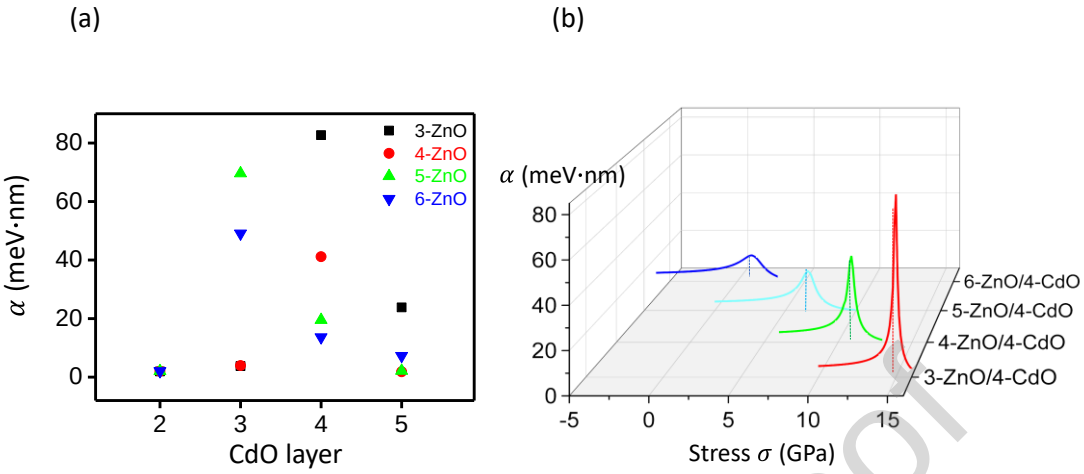

Figure 3

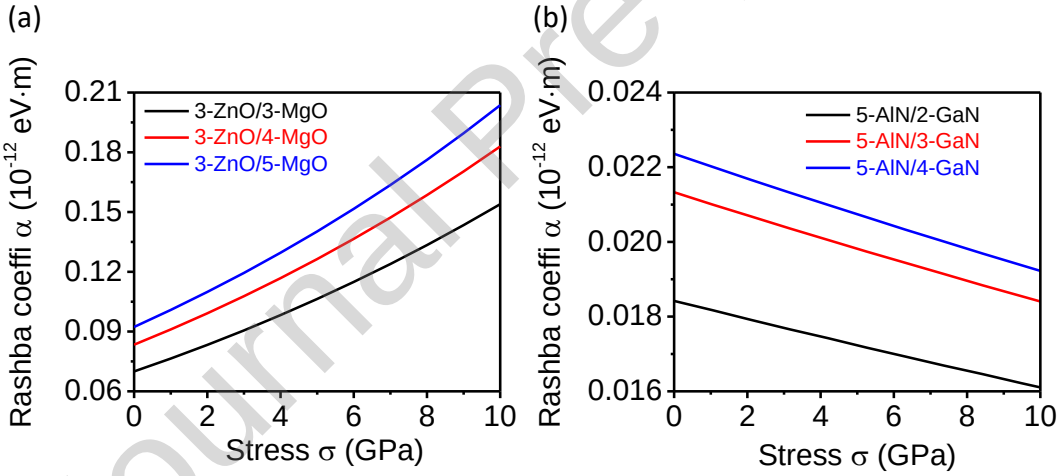

Figure 4

Table I

Rashba SOC coefficient α (meV · nm)	
GaAs/AlGaAs QW	0.05 [52]
GaN/AlGaN QW	0.15 [53]
GaN/InGaN QW	0.26 [29]
InAs QW	4.7 [47]
ZnO/CdO QW	82.7 (Present)

CRediT authorship contribution statement

Conceptualization: **YZ**; Data curation and Methodology: **MF, MD, GH**; Results analysis and discussion: **YZ, MF, MD, GH, LL**; Writing – original draft, review & editing: **YZ, MF, MD, GH, LL**.

Declaration of Competing **Interest**

☒ The authors declare that they have no known competing financial interests or personal relationships that could have appeared to influence the work reported in this paper.

☐The authors declare the following financial interests/personal relationships which may be considered as potential competing interests:

We wish to confirm that there are no known conflicts of interest associated with this publication and there has been no significant financial support for this work that could have influenced its outcome.
We confirm that the manuscript has been read and approved by all named authors and that there are no other persons who satisfied the criteria for authorship but are not listed. We further confirm that the order of authors listed in the manuscript has been approved by all of us.
We confirm that we have given due consideration to the protection of intellectual property associated with this work and that there are no impediments to publication, including the timing of publication, with respect to intellectual property. In so doing we confirm that we have followed the regulations of our institutions concerning intellectual property.
We understand that the Corresponding Author is the sole contact for the Editorial process (including Editorial Manager and direct communications with the office). He/she is responsible for communicating with the other authors about progress, submissions of revisions and final approval of proofs. We confirm that we have provided a current, correct email address which is accessible by the Corresponding Author and which has been configured to accept email from zhangyan@uestc.edu.cn
Signed by all authors as follows:

Yan Zhang

Lijie Li

Minjiang Dan

Mandun Fu Gongwei Hu

Highlights:

- Rashba spin-orbit interaction (RSOI) of ZnO/CdO quantum well (QW) has been investigated.
- Strain induced polarization of the QW adjusts the RSOI coefficient.
- A maximum RSOI coefficient appears when varying external stress.
- Ultrahigh RSOI coefficient has been unveiled by comparing a set of heterostructural QWs.